

*Hubble Space Telescope Imaging of the Binary Nucleus of the Planetary Nebula EGB 6*¹

James Liebert², Howard E. Bond³, P. Dufour⁴, Robin Ciardullo⁵, Michael G. Meakes⁶,
Alvio Renzini⁷, and A. Gianninas⁸

Received _____; accepted _____

ApJ, in press

¹Based on observations made with the NASA/ESA *Hubble Space Telescope (HST)*, obtained by the Space Telescope Science Institute. STScI is operated by the Association of Universities for Research in Astronomy, Inc., under NASA contract NAS5-26555.

²Steward Observatory, University of Arizona, Tucson AZ 85721; jamesliebert@gmail.com

³Department of Astronomy & Astrophysics, Pennsylvania State University, University Park, PA 16802; Space Telescope Science Institute, 3700 San Martin Drive, Baltimore, MD 21218; Current address: 9615 Labrador Ln., Cockeysville, MD 21030; bond@stsci.edu

⁴Département de Physique, Université de Montréal, C.P. 6128 Succ. Centre-Ville, Montréal, Québec H3C 3J7, Canada; dufourpa@astro.umontreal.ca

⁵Department of Astronomy & Astrophysics, Pennsylvania State University, University Park, PA 16802; rbc@astro.psu.edu

⁶Space Telescope Science Institute, 3700 San Martin Dr., Baltimore MD 21218; current address: 1717 Wilson Point Rd., Middle River, MD 21220; mgmeakes@gmail.com

⁷Osservatorio Astronomico di Padova, Vicolo dell'Osservatorio 5, I-35122, Padova, Italy; alvio.renzini@oapd.inaf.it

⁸Homer L. Dodge Department of Physics and Astronomy, University of Oklahoma, 440 W. Brooks St., Norman, OK 73019; alexg@nhn.ou.edu

ABSTRACT

EGB 6 is an ancient, low-surface-brightness planetary nebula. The central star, also cataloged as PG 0950+139, is a very hot DAOZ white dwarf with an apparent M dwarf companion, unresolved from the ground but detected initially through excesses in the *JHK* bands. Its kinematics indicate membership in the Galactic disk population. Inside of EGB 6 is an extremely dense emission knot—completely unexpected since significant mass loss from the white dwarf should have ceased $\sim 10^5$ yr ago. The electron density of the compact nebula is very high ($2.2 \times 10^6 \text{ cm}^{-3}$), as indicated by collisional de-excitation of forbidden emission lines. *Hubble Space Telescope* imaging and grism spectroscopy are reported here. These resolve the white dwarf and apparent dM companion—at a separation of $0''.166$, or a projected 96_{-45}^{+204} AU at the estimated distance of 576_{-271}^{+1224} pc (using the *V* magnitude). Much to our surprise, we found that the compact emission nebula is superposed on the dM companion, far from the photoionizing radiation of the white dwarf. Moreover, a striking mid-infrared excess has recently been reported in *Spitzer*/IRAC and MIPS bands, best fit with two dust shells. The derived ratio $L_{\text{IR}}/L_{\text{WD}} = 2.7 \times 10^{-4}$ is the largest yet found for any white dwarf or planetary nucleus. The compact nebula has maintained its high density for over three decades. We discuss two possible explanations for the origin and confinement of the compact nebula, neither of which is completely satisfactory. This leaves the genesis and confinement of the compact nebula an astrophysical puzzle, yet similar examples appear in the literature.

Subject headings: white dwarfs – planetary nebulae – binaries: visual – stars: individual (PG 0950+139) – planetary nebulae: individual (EGB 6, Tol 26, WeBo 1, A 70)

1. Introduction: The Bizarre Nucleus of EGB 6

1.1. A Compact Nebula around the Central Star

EGB 6 (PN G221.6+46.4, J2000: 09 52 58.99, +13 44 34.9) is a large ($13' \times 11'$) and very low-surface-brightness planetary nebula (PN). It was serendipitously discovered by one of us (H.E.B.) in 1978, during examination of Palomar Observatory Sky Survey (POSS) prints. The object was included in a list of faint nebulae found on POSS prints published by Ellis, Grayson, & Bond (1984, hereafter EGB). An extremely blue, 16th-mag planetary nebula central star (CSPN) is visible near the center of EGB 6. As described by EGB, a spectroscopic observation revealed the surprising result that the nucleus has strong [O III] emission lines. The central star was detected independently as a faint high-latitude blue star in the Palomar Green Survey (Green, Schmidt, & Liebert 1986), designated PG 0950+139; this was found to be a very hot DA white dwarf (WD) by Fleming, Liebert, & Green (1986). Spectroscopic observations by both groups of authors found that the emission lines from the CSPN arise from an unresolved compact emission nebula (CEN) component—a startling result, given that the large post-asymptotic-giant-branch age of the WD and EGB 6 would imply that significant mass loss from the nucleus should have ceased long ago ($\sim 10^5$ years). Note that this approximate age is appropriate to the oldest known PNe, and results from matching the slow kinematic velocity (~ 10 km/sec) with the large size (a few parsecs) of the oldest PNe. The CEN, in addition to being confined to the central part of EGB 6, is far too strong to be associated with the extremely faint outer PN, which to our knowledge has not been observed spectroscopically. Deep CCD images of EGB 6 have been published by Jacoby & van de Steene (1995) and Tweedy & Kwitter (1996).

In a comprehensive study of the CEN by Liebert et al. (1989, hereafter L89), the mystery intensified with the development of quantitative results. The very hot WD/CSPN is of type DAOZ, with a hydrogen-rich atmospheric composition, but with He II 4686 Å

appearing in absorption in the optical spectrum. Lines of heavier elements were found in the ultraviolet by Gianninas et al. (2010, hereafter G10), who published *FUSE* far-ultraviolet spectra revealing ions such as C IV, N IV, O VI, P V, S VI, Si IV, and Fe VI–VII in the spectrum.

In a study of hot WDs from the PG Survey by Liebert, Bergeron, & Holberg (2005), the derived parameters for the central star of EGB 6 were $T_{\text{eff}} = 108,390 \pm 16,687$ K and $\log g = 7.39 \pm 0.38$. However, the model atmospheres used in that study assumed a pure hydrogen composition and local thermodynamic equilibrium (LTE). Since helium and heavier metals appear in the spectrum, and non-LTE effects are almost certainly important at $T_{\text{eff}} \simeq 100,000$ K, this analysis needed to be redone. Taking these into account has always caused T_{eff} to be decreased. Sure enough, G10 fit the spectrum with non-LTE atmospheres, determining $T_{\text{eff}} = 93,233$ K, $\log g = 7.37$, and $\log(\text{He}/\text{H}) = -1.60$, assuming also the presence of C, N, and O at solar abundances. (No attempt was made to determine actual abundances of elements heavier than helium in their study.) G10 determined an estimated absolute magnitude $M_V = +7.0$ (see their Table 2). We revisit the absolute magnitude, and estimate the distance in §3.3, showing that both are quite uncertain.

The WD has a measured proper motion in the UCAC4 catalog (Zacharias et al. 2012) of $\mu_\alpha = 0''.0148 \text{ yr}^{-1}$, $\mu_\delta = 0''.0023 \text{ yr}^{-1}$. At the rough estimated distance of 576 pc, this object has a tangential velocity of about 40 km s⁻¹. L89 reported radial-velocity measurements from MMT echelle spectra of $+6.2 \pm 1.8$ (for He II 4686 Å) and $+19.2 \pm 9.4$ km s⁻¹ (for H α). Using a weighted mean of $+6.7$ km s⁻¹ for the radial velocity, we estimate a Galactic space motion relative to the local standard of rest of $U, V, W = +28.2, +11.8, -14.8$ km s⁻¹. At the likely distance of ~ 400 pc above the Galactic plane (at Galactic latitude 46.4°), this is an old Galactic disk object, as concluded by L89.

L89 showed that the CEN has the nearly unique property that the [O III] lines are

partially quenched, and the expected [O II], [N II], and [S II] forbidden lines are totally absent, due to collisional de-excitation at the very high density. This requires an electron density in excess of 10^6 cm^{-3} , making the CEN near the center of the old PN EGB 6 one of the densest known ionized hydrogen nebulae. However, as discussed later, another compact and apparently similar nebula—Tol 26, studied by Hawley (1981)—is even denser. Dense compact nebulae can also occur in the early post-asymptotic giant phase and in symbiotic stars.

The parameters of the EGB 6 CEN were estimated in more detail, using a photoionization model, by Dopita & Liebert (1989, hereafter DL). The CEN was found to have a mean density of $n_e = 2.2 \times 10^6 \text{ cm}^{-3}$ and a very small filling factor of $\log f \simeq -3.44$. From the observed line fluxes, DL concluded that the CEN is ionization-bounded, with an ionized mass of only $7 \times 10^{-10} M_\odot$. The radius of the Strömgren sphere was found to be only 38 AU ($1.23 \times 10^{10} \text{ km}$), assuming that it surrounded the WD. The line widths from echelle spectra covering $\text{H}\alpha$ and He II 4686 Å showed single, narrow-line components, implying an upper limit to any expansion rate of the nebula of 50 km s^{-1} .

DL speculated (several years before the first discoveries of “hot Jupiters” around nearby stars) that the CEN around the nucleus of EGB 6 might arise by ablation of a Jovian planet located within a few AU from the WD. While the hypothetical planet would have a radius similar to a low-mass dwarf star, its escape velocity at a Jupiter mass would be an order of magnitude lower, and of the same order of magnitude as the thermal velocities of photoionized material on the hot side facing the WD. However, this idea turned out to be incorrect.

1.2. A Cool Companion of the Hot Nucleus

Near-IR (NIR) photometry of EGB 6 by Zuckerman, Becklin, & McLean (1991) detected an appreciable IR excess in the K band over the Rayleigh-Jeans tail of the WD—with a coarse measurement of $K = 15.3 \pm 0.2$ —which they attributed to an M dwarf stellar companion. Fulbright & Liebert (1993) confirmed the excess NIR fluxes, finding $J = 16.43 \pm 0.20$, $H = 16.08 \pm 0.09$, and $K = 15.63 \pm 0.04$ (mean of multiple observations). These may be compared to the calculated magnitudes of the WD of $J = 17.60 \pm 0.62$, $H = 16.78 \pm 0.19$, and $K = 15.98 \pm 0.07$. These authors searched for variability over an interval of 30 days, in order to test the possibility that, instead of a normal M dwarf companion, the WD had a substellar or Jovian-mass companion so close that it was being heated on its facing side by ultraviolet radiation from the WD. In this case, the expected orbital period would be hours to at most a few days. However, no variability was detected.

Note that Wachter et al. (2003) reported $J = 16.43 \pm 0.114$, $H = 15.555 \pm 0.144$, and $K_s = 15.350 \pm 0.151$ from the Two Micron All Sky Survey (2MASS). The 2MASS measures agree well at J , but poorly at H and K_s . The 2MASS K_s band has a shorter long-wavelength cutoff than the standard Johnson K band. Moreover, the detection of variability at mid-IR (MIR) wavelengths (see the next subsection; Su et al. 2011) could imply variability also at the K and possibly the H band. However, the variability in H of 0.525 mag is greater than the difference of 0.28 between the mean K of Fulbright & Liebert (1993) and the 2MASS K_s value. The latter would arguably be less enhanced by an increased MIR excess. So we are left with no clear explanation of the changes in H and K .

It thus appeared likely that the WD has an ordinary M dwarf companion, although to our knowledge no IR spectrum has been obtained to confirm this. Using the accurate K -band measurement, at an estimated distance assumed at that time to be 450 pc, Fulbright & Liebert (1993) inferred an absolute $M_K = +7.7 \pm 0.7$, suggestive of a companion

of spectral type dM3.5–dM5. At the larger but uncertain 576_{-271}^{+1224} pc estimate (using the V magnitude), it is difficult to estimate the spectral type of the apparent dM companion. Moreover, the K magnitude is apparently variable. Using relations from Veeder (1974) for low-velocity main-sequence stars, we do note that a spectral type of M4 V would correspond to an $M_{\text{bol}} = +9.2$.

1.3. Dust Components

More recently, EGB 6 has been observed with *Spitzer* by Chu et al. (2011). They found striking MIR excesses, in all four IRAC bands, and with MIPS at $24\ \mu\text{m}$, at levels nearly four orders of magnitude greater than the extrapolated WD photosphere—§ 4. Bilíková et al. (2011, 2012) showed that the infrared excess extends beyond $35\ \mu\text{m}$, and has temporal variations on a timescale of a year. The contribution of the M dwarf at these MIR wavelengths is expected to be minor.

The MIR excess was best modeled with two dust shells of 500 K and 150 K, with a combined $L_{\text{MIR}}/L_{\text{WD}} = 2.7 \times 10^{-4}$ —Chu et al. (2011), excluding the contribution of the M dwarf. This is the largest IR excess found by these authors in a survey of many PN nuclei and hot WDs. Assuming an estimated distance of 647 pc, they calculated $L_{\text{IR}}/L_{\text{WD}} = 0.026$ and $0.025 L_{\odot}$, or $L_{\text{IR}}/L_{\text{WD}} = 2.68 \times 10^{-4}$ and 2.60×10^{-5} for the cool and warmer shells, respectively (Bilíková et al. 2012). The emitting areas of the shells are 15 and $0.12\ \text{AU}^2$, respectively.

Even more remarkably, Su et al. (2011) discuss variations in this MIR excess on a timescale of a year. A followup observation with the *IRS* spectrograph shows that the dust continuum is detected out to a wavelength of $35\ \mu\text{m}$ (Chu et al. 2011). As noted earlier, it is likely that the flux at K and H contribute to the high-frequency tail of this MIR

component—see Figure 2 of Chu et al. (2011).

Su et al. (2011) also discuss an observation of the CEN of EGB 6 obtained with the echelle spectrograph on the Kitt Peak 4-m Mayall telescope. The partially quenched [O III] 5007 Å profile shows a double-peaked component, although the H α and H β lines show only single peaks. The weaker [O III] 4959 Å probably also shows a doubled structure, and it is unclear what to conclude from the weak He I 5876 Å profile. The full widths at half maximum (FWHMs) of all lines measured in the echelle spectrum appear to be basically the same. The L89 MMT echelle observations of H α and He II 4686 Å were also single-peaked, with similar FWHM to the 4-m echelle values. The doubling of the forbidden oxygen transitions may be a radiative-transfer effect, indicating that the collisional de-excitation is greatest near the line center. If instead the [O III] profile were showing two velocity peaks, the same effect would presumably have been seen in the permitted lines. This proposed explanation needs to be tested by radiative transfer calculations also addressing the role of thermal broadening.

It was our hope in the early 1990s that additional clues to solving the mysteries of the CEN component might be obtained from high-resolution imaging with the *HST*, even with its compromised capabilities at that time due to spherical aberration. In § 2 our imaging results are presented, and we show that the CEN is detected as a resolved point-source companion of the WD that coincides with the apparent position of the dM star. In § 3 recent optical spectra spanning another two decades are reported, and equivalent widths of emission lines from the CEN are compared with prior values. In § 4 the puzzling *Spitzer* infrared observations are reviewed. In § 5 we attempt the daunting task of explaining the observations. Conference papers summarizing some preliminary conclusions of our study have appeared in Bond et al. (1992, 1993, 2009), Bond (1993), and Liebert et al. (2013).

2. Imaging Observations with HST

We obtained five sets of *HST* images and grism spectroscopy between 1991 and 1995, as summarized in the observing log in Table 1. The first sequence of observations was obtained in 1991, using the aberrated telescope with the Faint Object Camera (FOC) in its f/96 mode. The narrow-band F486N and F501N filters were used, to isolate the emission lines of $H\beta$ and [O III] 5007 Å, respectively. At the time of these observations, our aim had been to test the Jovian-planet hypothesis of DL, in which case the CEN would essentially coincide with the hot central star. To our surprise, we instead resolved the system into two separate star-like objects, as depicted in the top row of images in Figure 1. The fainter component, brighter in [O III] 5007 Å, lies almost directly west of the primary star at separation measured initially to be $0''.173$.

We used the “imexamine” task in IRAF¹ to perform simple aperture photometry in order to measure the magnitude differences between the two components; the results, which are only approximate because the companion lies in the wings of the aberrated images of the primary, are 2.3 and 1.3 mag, in $H\beta$ and [O III] respectively. We may compare these to the predicted magnitude differences between these two emission lines and the continuum of the hot WD, as follows. The equivalent widths of $H\beta$ and [O III], given in Table 2C of L89, are 2.9 and 17.9 Å, respectively. The FWHM widths of the F486N and F501N filter bandpasses are 34 and 74 Å (Nota et al. 1996). Thus the expected magnitude differences are roughly $-2.5 \log(2.9/34) = 2.7$ and $-2.5 \log(17.9/74) = 1.5$. The rough agreement with the observations shows that, at this level of approximation, essentially all of the emission-line fluxes are located with the apparent companion dM object, and not from the hot WD!

¹IRAF is distributed by the National Optical Astronomy Observatories, which are operated by the Association of Universities for Research in Astronomy, Inc., under cooperative agreement with the National Science Foundation.

In 1993 February, in order to explore the relationship of the resolved CEN source to the putative dM companion star, we obtained broad-band images of EGB 6 with the original aberrated Wide Field and Planetary Camera (WF/PC1) on *HST* in the high-resolution Planetary Camera mode. We used the F555W (“V”) and F785LP (“I”) filters. The second row of pictures in Figure 1 depicts these images. In a separate “Snapshot” program (described in detail by Ciardullo et al. 1999), in 1993 December, we observed EGB 6 again with WF/PC1 in the same filters; these images are very similar to those illustrated in Figure 1 and are not shown separately. In these broad-band images, we clearly detect a stellar companion, at the same separation and position angle as the emission-line source. As the middle row in Figure 1 shows, the companion is very red, being much brighter in the *I* band than in *V*. We conclude that this red source is the dM companion that is the source of the NIR excess, and that the CEN is associated with this object rather than the nearby hot WD. The source is also weakly detected in F555W, but this filter transmits both $H\beta$ and the [O III] emission lines, which plausibly account for the signal at *V*.

The magnitude difference between the *I*-band companion and the WD is approximately 1.2 mag, but this is uncertain because the companion unfortunately lies on the first Airy diffraction ring of the WD primary. Roughly speaking, due to the large uncertainty in distance, the red companion has $M_I \simeq +8.4 \pm 1.6$, in approximate agreement with the conclusions about the red companion outlined in § 1.2, based independently on the *JHK* excess.

In order to verify the remarkable finding that the CEN is entirely separated from the hot WD, in 1993 April we made low-dispersion slitless spectroscopic observations with WF/PC1 in its grism mode. Dispersed images were obtained with the G450L (covering the interval 3000–6000 Å at a dispersion of 25 Å pix⁻¹) and G800L (6000–10000 Å, 51 Å pix⁻¹) grisms. We selected a telescope roll angle that placed the dispersion perpendicular to the

line joining the two point-like sources, thus maximizing their spatial separation. Figure 2 is a pictorial representation of the grism spectra. In the G450L image, the companion is detected only in the [O III] 4959 and 5007 Å emission lines (Figure 2 left panel; the much weaker H β line is not detected in these exposures). The emission features are separated from the bright continuum of the WD by the same angular amount as in the direct images. In the G800L frame (Figure 2 right panel) we see flux from the companion only at the H α emission line. At first glance, the companion appears also to have a “pseudo-continuum” in both images; however, these apparent continua are artifacts produced by the Airy ring of the bright WD, as demonstrated by the fact that their separation from the WD increases proportionally to wavelength, as well as the fact that there are identical artifacts symmetrically placed on the east side of the WD.

There are no detectable emission lines in the spectrum of the hot WD or its immediate environment. As a further test, we determined a very approximate equivalent width (EW) for the combined flux from [O III] 4959 and 5007 Å relative to the adjacent WD continuum. This measurement is very crude because of the superposed Airy ring, but subtracting it approximately from the line flux yields a total EW of 18 Å. This is in quite reasonable agreement, given the uncertainties, with the total of 23.3 Å measured from calibrated slit spectra of the combined light of both components (Table 2C in L89). We conclude that the entire CEN flux comes from the immediate vicinity of the dM companion, and not from the hot central star.

Our final *HST* imaging of EGB 6 was done in 1995 October, in a continuation of our snapshot program on planetary nuclei. These observations were done with the non-aberrated Wide Field Planetary Camera 2 (WFPC2) and F555W (“V”) and F814W (“I”) filters. Pictorial representations of these images are shown in the bottom row of Figure 1. The faint companion of the CSPN is weakly detected in both images. As before,

the V detection is most likely due to the fact that the F555W filter transmits the $H\beta$ and [O III] emission lines. The red companion is detected in the I band, but more weakly than in the earlier WF/PC1 F785LP image shown in Figure 1. This apparent discrepancy is likely due to the fact that the WFPC2 F814W band pass cuts off sharply near 9600 \AA , whereas the WF/PC1 F785LP bandpass transmits up to about $1.1 \mu\text{m}$. Examination of Fig. 3 of Fulbright and Liebert (1993) suggests that the excess of the dM companion over the declining WD continuum turns on sharply near or slightly below $1 \mu\text{m}$ —see also Fig. 2 of Chu et al. (2011). Thus the stronger detection of the companion with the WF/PC1 I filter than with WFPC2 is consistent with its very red color.

We carried out astrometry of the *HST* images, using the centroiding tool in IRAF’s “imexamine” task, and conversion to right ascension and declination with the “xy2rd” task. The results are given in Table 2. The companion was not detected well enough in the 1993 December snapshot frames (which were single exposures, rather than the pairs of frames taken at the other WF/PC1 and WFPC2 epochs for cosmic-ray removal), so this epoch is omitted. The internal errors of the astrometry are of the order of a few milliarcseconds, but it is difficult to estimate the systematic errors due to the aberrated images at the first two epochs, and the fact that the companion lies in the Airy ring of the primary star. The errors listed in Table 2 were estimated from the scatter among the three independent measurements (thus tacitly assuming no significant orbital motion of the companion from 1991 to 1995—a reasonable assumption for the nominal orbital period estimated below—as well as assuming that the emission-line object coincides exactly with the dM star).

The mean of the measurements (giving double weight to the FOC data) is a separation of $0''.166$ and a J2000 position angle of $267^\circ.8$. At the estimated distance of 576_{-271}^{+1224} pc, this corresponds to a projected separation of 96_{-45}^{+204} AU, and a nominal orbital period (for assumed masses of 0.6 and $0.2 M_\odot$) of about 1200 yr. The linear dimensions of the

surrounding faint, large PN (EGB 6) are approximately 2–2.5 pc.

3. Optical Spectra of EGB 6 Obtained Since 1988

The available spectroscopic observations of EGB 6 from 1978 through 1987 were presented by L89. In this section we discuss two observations obtained by us in subsequent years. The main purpose was to extend the time baseline in a search for spectrum variability of the CEN that might arise from changes in nebular density.

3.1. 1992 MMT Spectrum

On 1992 December 27 we used the old Smithsonian-Arizona Multiple Mirror Telescope (MMT, at that time with six 72-inch mirrors) and red-channel spectrograph to observe EGB 6 with an 800×1200 Loral CCD detector and a $600 \text{ grooves mm}^{-1}$ grating covering $3650\text{--}5250\text{\AA}$ at 6\AA resolution. A long slit was used, but no record of the slit width or positional orientation has survived for this 20-year-old observation. It was noted, however, that three spectra were obtained under less-than-ideal weather conditions, and were combined to achieve a continuum signal-to-noise (S/N) ratio near 80. Because the conditions were non-photometric, no absolute line fluxes were determined. This spectrum is similar to prior published spectra, except for the lower spectral resolution and higher S/N. Unfortunately with no digital record, we cannot apply the method used in the next subsection to subtract the photospheric continuum of the modeled WD spectrum, published in 2010.

No significant variation in the relative strengths of the forbidden lines compared to those reported in L89 was found. In particular, the ratio of the three [O III] lines is very density-sensitive in the high-density regime found in this object. The ratio

$R([\text{O III}]) = [I(5007 \text{ \AA}) + I(4959 \text{ \AA})]/I(4363 \text{ \AA})$ in the 1992 observation is identical to the value of 12.9 from the mean values of the 1978–1987 observations from Table 2C of L89. Arguably the most photometric measurement in L89 was the original IIDS observation made by H.E.B. with the Kitt Peak 2.1-m telescope on 1978 April 11, using a $4''3$ circular aperture; this observation gave $R([\text{O III}]) = 12.6$, not a significantly different value. The time span is 14 years between these measurements.

The $[\text{Ne III}]$ 3868.8 Å line is not significantly different (based on the EW) between the measurements of L89 (1.7 Å) and 1992 (1.9 Å). The critical density for this transition listed in Osterbrock (1989, see Table 3.11) should also be low enough for collisional de-excitation of $[\text{Ne III}]$ to occur at the DL nebular density. $[\text{Ne III}]$ 3868.8 Å and 3967.5 Å correspond to $[\text{O III}]$ 4959 and 5007 Å while the so-far unobserved $[\text{Ne III}]$ 3342.5 Å line corresponds to $[\text{O III}]$ 4363 Å. The neon ratios can similarly be measured as another test of the electron density.

3.2. 2007 MMT Spectrum

The CEN presents a problem in determining the absolute strengths of the Balmer and helium emission lines from ground-based spectra, because they are superposed on photospheric absorption lines in the WD spectrum. The best model-atmosphere fit to the WD spectrum is that of Gianninas et al. (2010), which is the first non-LTE analysis including CNO and helium abundances. The model’s synthetic spectrum gives us a tool to remove the photospheric contamination of the CEN spectrum. A newer spectrum from the MMT, now a 6.5-m single-mirror telescope, was obtained on 2007 December 15. The spectrograph, with a $500 \text{ grooves mm}^{-1}$ grating and one arc-second slit, achieved 4 Å resolution. However, the sky was partly cloudy, which stopped us from observing at times during the night, so absolute fluxes could not be measured.

The top panel in Figure 3 shows this spectrum. The synthetic spectrum from the best-fitting WD model of Gianninas et al. was then subtracted, in order to obtain the CEN spectrum shown in the bottom panel of Figure 3. The subtraction of the model spectrum produced clean nebular line fluxes, with no residual continuum, except for a slight “negative” apparent flux in the 3900–3950 Å region.

Table 3 presents the CEN fluxes, both the adopted values from L89 (corrected for a typographical error in the caption of the L89 Table 2C), and from the 2007 MMT observation. The fluxes are presented in units of 10^{-15} erg cm $^{-2}$ s $^{-1}$ for (1) the quoted mean L89 values (with no photospheric absorption corrections), and (2) those measured from the 2007 MMT observation, plotted in the bottom panel of Figure 3, with correction for the WD absorption. Note that the H α flux from the earlier measurements is affected rather little by the weaker absorption line from the photosphere because the H α emission is relatively strong. The ratio of H α /H β is 2.67 from the mean L89 flux values, but the value of H β is diminished by stronger photospheric absorption than is H α . The ratio is close to the value of 2.81 which is expected from an optically thick (Case B), ionized hydrogen gas of 10,000 K, $n_e = 10^6$ cm $^{-3}$, the closest among the Tables 4.2–4.4 from Osterbrock (1974) to the T_e and n_e values determined by DL. The H γ /H β and H δ /H β flux ratios (to two significant digits) of 0.47 and 0.25 from the cleanest emission spectrum of 2007 compare with 0.471 and 0.262 from this same Osterbrock case. Since H ϵ is blended with the even stronger [Ne III] 3967.5 Å emission line, H ϵ must be omitted from the discussion of ratios. Finally, H8 (3889.1 Å) and H9 (3835 Å) also show the normal downward progression in strength relative to H β . (Note that L89 did not comment on the higher Balmer emission lines, presumably because of their weakness against the WD photospheric absorption.)

Note that the actual n_e is over a factor of two higher and the T_e of 11,400 K is over 10% higher, but the dependence of the ratios on n_e and T_e are modest. The Balmer line

ratios thus indicate that very little reddening affects the CEN.

Some peculiarities are apparent in Table 3 and Figure 3. First, the 2007 fluxes are lower than those in L89 by an approximately constant factor of ~ 0.75 . This likely indicates an error in the absolute flux calibration of one (or both) of the observations, but the line intensity ratios would remain reliable.

There is a broad apparent dip in absorption with a sharper dip near 3930 \AA seen in Figure 3. It is implausible for this to be interstellar extinction, given the tight constraints on reddening shown in L89 (their § 2). This apparent absorption dip is due to imperfect subtraction of the WD synthetic spectrum.

The $R([\text{O III}])$ value for the 2007 observation is 9.8, apparently lower than the values of ~ 12.9 in L89 and in 2002. Note, however, that the value of R is very sensitive to the weak $[\text{O III}] 4363 \text{ \AA}$ line, which was probably effectively weakened by a blend with the photospheric $\text{H}\gamma$ absorption line in the earlier spectra, making the value of R too high. There is thus no strongly compelling evidence for significant changes in the CEN spectrum over the 1978–2007 interval. Moreover, the equivalent widths of the emission lines, i.e., normalized to the continuum of the WD and independent of calibration zero-points, have not changed significantly during this three-decade interval.

3.3. Model-Atmosphere Fit

We now revisit the G10 fit, which used the spectrum discussed in the preceding subsection. Figure 4 shows a more detailed display. The cores of the weak H and He II absorption lines of the WD are contaminated by the strong, narrow emission lines of the CEN. The detailed plot of individual line fits in the left panel of the figure shows how difficult and inaccurate the fit is. The surface gravity with correct error bar is

$\log g = 7.37 \pm 0.79$ —see Fig. 23 of G10. The same figure shows that T_{eff} is also uncertain by $\sim 20,425 \text{ K}^2$.

These values were used to compute the absolute magnitude in the V and Sloan Digital Sky Survey (SDSS) g -bands, respectively, using the photometric calibrations of Holberg & Bergeron (2006). These are $M_V = +7.22 \pm 1.64$ and $M_g = +6.86 \pm 1.64$. By coupling these absolute magnitudes with the observed $V = 16.025 \pm 0.025$ (EGB) and $g = 15.66 \pm 0.04$, respectively, we computed spectroscopic distances of 576_{-271}^{+1224} and 585_{-276}^{+1243} pc. (We arbitrarily adopted the former value in some calculations herein.) Though these distances are quite uncertain, they are at least consistent within the computed error bars.

4. Constraints from the Mid-Infrared Excess

As discussed in § 1.3, EGB 6 shows a MIR excess. The *Spitzer* IRAC and MIPS fluxes of EGB 6, listed in Chu et al. (2011), at wavelengths of $3.6 \mu\text{m}$, $4.5 \mu\text{m}$, $5.8 \mu\text{m}$, $8.0 \mu\text{m}$, and $24 \mu\text{m}$ are respectively 977 ± 15 , 1176 ± 15 , 1773 ± 36 , 3772 ± 37 , and $11740 \pm 66 \mu\text{Jy}$. These authors note similarities to the MIR excess in the Helix PN, with an age of $\sim 10^4$ yr (O’Dell et al. 2002). The *Spitzer* MIPS observations of the Helix show a bright compact source in the 24 and $70 \mu\text{m}$ bands (Su et al. 2007).

For EGB 6, there is no indication of significant extinction in the ultraviolet and optical fluxes of the hot star and the CEN. For the star, L89 found that the *IUE* plus optical *UBV* fluxes fit a power law of the following form (F_λ in cgs units, λ in \AA):

²The uncertainty in T_{eff} was mistakenly reported as 425 K in Gianninas, Bergeron, & Ruiz (2011).

$$\log F_\lambda = -3.65 \log \lambda - 1.175.$$

This was steeper than that of the well-studied 50,000 K DA WD G 191-B2B (slope -3.59). The conclusion was that there was no detectable extinction, with a limit of $A(1200 \text{ \AA}) < 0.2$ mag, corresponding to $E(B - V) < 0.02$ (Seaton 1979). This in turn corresponds to $N_{\text{H}} < 1.2 \times 10^{20} \text{ cm}^{-2}$, in the line of sight to the WD.

For the CEN the extinction constraint is weaker, since the Balmer emission line ratios are difficult to measure, being superposed on the absorption lines of the WD. Nonetheless, as noted earlier, L89 found that the $\text{H}\alpha/\text{H}\beta$ flux ratio is consistent with no detected extinction, as are the ratios of higher Balmer lines discussed in § 3.2.

For this line-of-sight position on the sky, Schlegel et al. (1998) estimate $A_V = 0.104$, implying $E(B - V) = 0.034$; this results from a reprocessed composite map of the *COBE/DIRBE* and *IRAS/ISSA* maps, with zodiacal foreground and confirmed point sources removed. Schlafly & Finkbeiner (2011) measure $A_V = 0.086$, implying $E(B - V) = 0.028$, using measurements of dust reddening from the colors of stars with spectra obtained by the SDSS. Here we used the tools provided by the NASA/IPAC Extragalactic Database (NED) for coordinate transformation and galactic extinction calculation. In both cases a standard ratio, $R = A_V/E(B - V) = 3.1$, was applied to convert to $E(B - V)$. Both estimates of $E(B - V)$ for this celestial position are again quite small, and apply to the total line of sight out of the Galaxy. Thus, there is no evidence that the source of the excess *Spitzer* MIR flux is in front of either the hot WD star or the CEN.

Assuming that the origin of the excess detected in the MIR is two shells or disks of dust, as fitted by Bilíková et al. (2012), we note that the surface areas—15 AU² for the 100 K shell, and 0.12 AU² for the 500 K shell—are large compared with the WD and putative M dwarf. Hence the column densities of dust in the respective lines of sight may not be

large enough to register detectable extinction in either case. This leaves undetermined the location of the presumed dust shells.

5. The Compact Emission Nebula (CEN)

5.1. Constraints on the Model

As stated in §2, the angular separation of $0''.166$ implies a lower-limit physical separation of the CEN from the WD of $a \simeq 96_{-45}^{+204}$ AU for the assumed distance of 576_{-271}^{+1224} pc. The DL filling factor, f , might now be interpreted instead as a covering factor—i.e., that the ionized gas sits in a large CEN coincident with the I -band and NIR dM component, intercepting a fraction f of the WD’s radiation. If spherical, and adopting the DL value of $f = 3.63 \times 10^{-4}$, the CEN would have a radius given by

$$R_{\text{CEN}} \simeq 2 a f^{1/2} \simeq 3.6 \text{ AU},$$

assuming the CEN to be optically thin in $\text{H}\beta$, as the fits to Case B of Osterbrock (1974) indicate. However, correcting for the distance now estimated to be 576_{-271}^{+1224} pc, the filling/ covering factor f will be $(6.4 \pm 3) \times 10^{-4}$. Now the above equation produces $R_{\text{CEN}} = (4.2 \pm 2) \times 10^8 \text{ km} = 4.8_{-2.3}^{+10.3} \text{ AU}$.

Note that this supergiant size is necessary in order for the CEN to intercept enough ionizing photons to produce the observed $\text{H}\beta$ flux (see L89).

However, since the CEN does not surround the WD, the simple steady-state mass-loss hypothesis envisioned by L89 and DL cannot apply. If in fact the excited gas were due to ongoing mass loss from the dM star, the CEN should be growing in size and in intercepted solid angle of radiation from the WD. This would cause the luminosity of the CEN to grow

with time, with its average density decreasing. If the CEN were formed from gas lost from the M dwarf, this would also lead to a time-varying nebula; the nebula would grow in size and decrease in density. However, as described in § 3, over three decades of observations have not revealed any changes in the emission-line spectrum.

Instead of a slowly expanding gaseous nebula recombining at the ionization boundary and replenished by mass loss from the host object, we are forced to invoke a scenario involving an essentially static CEN of extraordinarily high density—in comparison to standard H II regions and normal PNe (apart from the most compact, young proto-planetary nebulae, and a few peculiar objects like those discussed below in § 6). Note, however, that the emission-line widths are consistent with an expansion velocity of up to about 50 km s^{-1} . But, if from the nonvariability argument, we assume simply that the CEN has not doubled in size in over twenty years, an upper limit to the expansion velocity is $<1 \text{ km s}^{-1}$!

We now consider two hypothetical explanations for the existence of a CEN surrounding, or in the immediate vicinity of, the dM companion of the hot CSPN: (1) it is a region of compressed gas, created at the location where a fast wind from the WD collides with a slower wind from the dM star; or (2) it is a residual structure around the dM star, consisting of material captured from the PN outflow from the CSPN, and surviving to the present time.

5.2. The “Dueling-Winds” Model

Let us assume that both binary components are losing mass in the form of winds. As noted in the previous subsection, any such wind from either component is expected to have a velocity far in excess of the measured limit on the photo-ionized gas discussed in the previous section. Let us further hypothesize, however, that the faster WD wind encounters

that of the dM dwarf near the latter’s position in the binary system (as required by the imaging of the CEN component). Given sufficient mass fluxes and supersonic velocities, a shock may result which would greatly slow down both gaseous components. The density of the shocked gas can be much higher than the densities of either wind component because it is confined by the ram pressures of the two winds. This essentially static entity will then be photoionized by radiation from the WD.

The constraints on this model from the observations are:

(1). The ram pressures of the two winds are comparable to the pressure in the ionized gas, which is known from the ionization model to be

$$P_g = 3 n_H kT \simeq 1 \times 10^{-5} \text{ dynes cm}^{-2},$$

(using $n_H = 2.2 \times 10^6 \text{ cm}^{-3}$ and $T = 11,400 \text{ K}$).

(2). The projected separation of the binary is $a = 96_{-45}^{+204} \text{ AU}$, so the true separation is at least this much. Since this value and the systemic distance are uncertain, we shall scale to a binary separation of 100 AU in the calculations below.

(3). The covering factor of the ionized gas is also determined by the ionization model to be approximately $f \simeq 6.4 \times 10^{-4}$.

We can derive the product $\dot{M}_{\text{WD}} V_{\text{WD}}$ for the WD from the first two constraints, and the same product ($\dot{M}_{\text{dM}} V_{\text{dM}}$) for the companion using the third. For the WD

$$\begin{aligned} \dot{M}_{\text{WD}} V_{\text{WD}} &= 4\pi a^2 P_g / \beta \\ &= 6 \times 10^{25} \text{ g cm s}^{-2} \\ &= 1 \times 10^{-5} (a/100 \text{ AU})^2 M_{\odot} \text{ yr}^{-1} \text{ km s}^{-1}, \end{aligned}$$

or

$$\dot{M}_{\text{WD}} = 1 \times 10^{-9} M_{\odot} \text{ yr}^{-1} \left(\frac{10,000 \text{ km s}^{-1}}{V_{\text{WD}}} \right),$$

where β is the overpressure (approximately unity, or a bit larger) in the stagnation region between the shocks.

While there is no physical justification for such a high mass-loss rate from a hydrogen-rich WD, it probably cannot be entirely ruled out by observation. This model might be tested by high-resolution spectrophotometry covering the far-ultraviolet resonance lines. Ground-based echelle spectra covering He II 4686 Å and H α show single-component lines with no evidence for outflow, but these are not resonance lines.

To derive $\dot{M}_{\text{dM}} V_{\text{dM}}$ for the companion, we need to know how far from the dM star the shock is located. As noted in §5.1, the radius of the CEN is about $R_{\text{CEN}} \simeq 2 a f^{1/2} \simeq 4.8(a/100\text{AU}) \text{ AU}$.

If we make the plausible assumption that the dM wind shock occurs at a distance R_{cl} from the star, then

$$\begin{aligned} \dot{M}_{\text{dM}} V_{\text{dM}} &= 4f \dot{M}_{\text{WD}} V_{\text{WD}} \\ &= 1.4 \times 10^8 M_{\odot} \text{ yr}^{-1} \text{ km s}^{-1}, \end{aligned}$$

yielding

$$\dot{M}_{\text{dM}} = 1.4 \times 10^{-11} M_{\odot} \text{ yr}^{-1} \left(\frac{1000 \text{ km s}^{-1}}{V_{\text{dM}}} \right).$$

There are no recent estimates of the mass loss rate from M dwarfs, after an old, highly uncertain figure of $\sim 10^{-12} M_{\odot} \text{ yr}^{-1}$, ascribed to flaring M dwarfs (Coleman & Worden 1976), although Wood et al. (2001, 2002) present a much lower upper limit for the less active M5.5 V solar neighbor Proxima Centauri. Moreover, in the present case the existence of

a hot companion may enhance whatever spontaneous mass loss the M dwarf may sustain. Actually, we can turn around the issue, and claim that ours is a reasonable estimate for the current mass loss rate from this M dwarf companion to a hot white dwarf. Measuring mass loss rates from red giants is already a very uncertain exercise, while measuring it in M dwarfs looks to be totally hopeless.

There is one further argument that can be used to restrict \dot{M}_{dM} . The ionized gas must be flowing out of the compressed region between the wind shocks at roughly the thermal velocity, $v_{\text{ion}} \simeq 10 \text{ km s}^{-1}$. Therefore the timescale for the ionized gas outflow is

$$\tau_{\text{ion}} \simeq R_{\text{CEN}}/v_{\text{ion}} \simeq 2 \text{ yr} .$$

Balancing the mass input from the dM star wind with the mass output of the ionized gas, we have

$$\dot{M}_{\text{dM}} M_{\text{ion}}/\tau_{\text{ion}} \simeq 5 \times 10^{-10} M_{\odot} \text{ yr}^{-1} ,$$

based on the observed mass of ionized gas, $M_{\text{ion}} \simeq 7 \times 10^{-10} M_{\odot}$. Note that the mass loss rate is appreciably larger than the estimate two paragraphs ago, but that estimate was judged to be uncertain.

Finally, in § 4 we showed that the extinction in the lines of sight to the WD and CEN are small (undetectable). We assume that the CEN is produced where the two winds collide between the WD and dM, but closer to the latter. Let us hypothesize that the dust condenses out behind this nebula, where it is initially shielded from the hard radiation of the WD. However, as it spreads out, it will likely absorb WD flux and form a turbulent stream which drifts beyond the dM and CEN. Note that the dust does not lie in front of (the line of sight to) either the WD or dM in this scenario. It can then be heated by radiation from both components, as the dust is slowly driven by radiation pressure away from the WD. Such a hypothesis might produce the only component of this system that varies—the dust shell(s)—if the dust forms episodically, then drifts away.

5.3. A Residual Envelope or Circumstellar Disk around the M Dwarf

An alternative explanation for the CEN in the EGB 6 system was suggested by Zuckerman et al. (1991): that the dM star captured the amount of nebular mass cited above into an envelope or circumstellar disk, at the time of the PN ejection from the primary star. It is plausible to assume that a disk might form around the companion star, since the orbital motion imparts a net angular momentum to the outflowing gas (or it could also have a small amount of intrinsic angular momentum).

Jeffries & Stevens (1996) discuss a class of wide binaries containing hot WDs or CSPN and cool, rapidly rotating, magnetically active companions. Significant spin-up of the latter may occur, resulting in what they call a wind-induced rapidly rotating (“WIRRing”) star, along with the formation of a disk, and accretion of chemically enriched material from the AGB star. The detection of peculiar carbon and *s*-process elements such as barium that were present in the wind of the former-AGB star may thus provide an evolutionary link between WIRRing stars and barium giants. This phenomenon may explain the “Abell 35”-type PN nuclei, in which the hot CSPNs are accompanied by rapidly rotating cool companions (e.g., Bond, Ciardullo, & Meakes 1993). Note, however, that the component separation in EGB 6 is much larger than in the known barium binary stars, but this may simply be due to selection against finding such systems with much wider separations.

A good example may be WeBo 1 (PN G135.6+01.0), having a remarkable thin-ring morphology around a late-type giant with overabundances of carbon and *s*-process elements (Bond, Pollacco, & Webbink 2003). The giant is chromospherically active, a “spotted” WIRRing star with a 4.7-day rotation period. These authors surmised that the likely undetected CSPN is now a hot subdwarf or WD which polluted its companion, and spun up its rotation, during the PN ejection phase. The putative hot companion of the cool optical barium star in WeBo 1 has recently been detected directly through UV observations with

the *Swift* satellite (Siegel et al. 2012). Abell 70 is another PN that may be a similar case, where a cool, optical, barium-enhanced companion is detected along with the hot central star (Miszalski et al. 2011,2012). Mira B is a WD ~ 70 AU from the AGB primary, recently resolved by *HST* (Ireland et al. 2007). However, Mira B apparently has an optically thick circumstellar disk regularly being fed material from the mass-loss/wind—see Fig. 3 of Ireland et al. (2007).

These examples make it clear that an accretion disk can form around a companion to a PN nucleus (a former AGB star, now a WD), even at fairly large separations. However, the active PN-ejection phase typically lasts no more than a few times 10^4 years. Whether a dense disk or envelope around the late-type companion can survive for $\geq 10^5$ years is unclear. This is the evolutionary time estimated for the WD (L89), which is similar in order of magnitude to the likely kinematic expansion age of the extended PN of EGB 6.

Moreover, the required size of the presumed disk or CEN is again constrained by the covering factor to be several AU. This is implausibly large, compared with the sizes of disks normally associated with main-sequence stars.

If a captured circumstellar disk explains the CEN in EGB 6, then it is puzzling why other PN nuclei in which a low-mass companion orbits the CSPN at smaller separations than in EGB 6 do not show the same phenomenon. An example of such a system is BE Ursae Majoris, a short-period eclipsing binary located within a faint PN; this shows a spectacular emission line spectrum, with strong orbital variations due to the heating of the facing side of the companion (Ferguson et al. 1987). However, there is no evidence for mass loss or the formation of an ambient emission nebula. A series of spectra of BE UMa obtained during the 1990s (unpublished) both at minimum and near maximum light show no evidence for [O III] or [Ne III], the strong forbidden emission lines seen in the EGB 6 spectrum (Fulbright & Liebert 1993).

Finally, the origin of the dust shells must be in the outer part of the disk in this scenario. This places it in the line of sight to the secondary star, which might cause extinction, unless the dust torus were at high inclination to our line-of-sight. On balance, we favor the scenario of the previous subsection, the “duelling winds” model.

6. EGB 6: An Unsolved Problem of Stellar Evolution

We end this paper in an unsatisfactory way: no clear answers, only the accumulation of questions. Our study of this object is now entering its fourth decade, beginning with the discovery and first observations in the 1970s, and the publications of the discoveries by EGB in 1984 and the PG Survey in 1986. The mysteries seem only to compound.

With the launch of *Spitzer*, new observational results were introduced, which forced a reconsideration of the extant issues, but pose at least two new ones. What is the source of the MIR excess, detected in all IRAC bands and with MIPS and IRS? The simplest model is to introduce two dust shells of 150 and 500 K. But where is this dust located in or around the binary system? Why is there absolutely no evidence of extinction in front of the WD, and (somewhat less established) in front of the CEN? A residual shell complex on a much bigger scale applicable to a younger PN such as the Helix seems to be a possible explanation. However, the EGB nebular shell is much older than the Helix, yet the CEN is very much smaller. Perhaps the scenario outlined in § 5.1 is the best explanation.

It might be worthwhile to summarize the basic constraints on the model:

- 1) there is no variability, except for the assumed MIR-emitting dust shells.
- 2) the CEN is situated with the presumed dM companion star, which dominates the *JHK* flux, at least ~ 96 AU from the source of photoionizing radiation.

3) neither the WD nor CEN are appreciably reddened.

Point (1) implies a stationary configuration, with the CEN constantly replenished to compensate for its evaporation, on a timescale of order one year. Point (2) leads to an origin of the CEN in the colliding winds in between the two stars, but closer to the dM. Point (3) suggests that the MIR emitting dust is in front of neither the WD nor the CEN; hence its likely location is in a turbulent stream beyond the dM and the CEN. If the dust forms episodically, and later is lost from the system, this component could vary; this would account for the observed MIR flux variation.

Finally, we note that the “EGB 6 phenomenon”—a very dense, compact emission nebula (CEN)—is not unique. In a paper that pre-dated the publication of the EGB 6 CEN, Hawley (1981) studied a “peculiar emission line object” (1230–275, now designated Tol 26), found in a Curtis Schmidt survey at Cerro Tololo by Smith et al. (1976). Hawley showed that this CEN is even denser than the one in EGB 6 ($n_e = 4 \times 10^6 \text{ cm}^{-3}$), as indicated by the [O III] line ratios and the absence of the singly ionized forbidden O, N, and S doublets.

Frew & Parker (2010, their §4.7.1, entitled “EGB 6 and its Kin”) discuss several other PNe and related objects with unresolved compact, dense knots at their centers. The central stars are not always WDs. For example, PHR J1641–5302 has a nucleus classified WC4, a much more luminous star than in EGB 6. However, the nebula shows an $R([\text{O III}])$ value indicating high density, again with no [N II] or [S II] detected. The nature of the very red PHR 1757–1711 = PTB 15 (Boumis et al. 2003) is unclear, since [O III] 4363 Å was not measured; however, the emission nebula shows no [N II] or [S II]. NGC 6804 has a compact emission nebula coincident with the luminous CSPN (Bilíková et al. 2012). Finally, Miszalski et al. (2011) suggest that the EGB 6 nebula has evolved from an object like the PN M 2-29; this luminous object has shown an R Coronae Borealis-like fading event in its

light curve, triggering a dust/cloud formation event.

Thus, Nature has been able to reproduce what seem like very unusual physical conditions at least a few times.

7. Suggested Further Observations

In lieu of having clear answers, we now mention some future work which can result in some clarification:

(1) An *HST*/STIS spectrum of the resolved WD could produce much-improved stellar parameters, especially the surface gravity and absolute magnitude, and the spectrophotometric distance measurement. A measurement of the distance by the European Space Agency *Gaia* mission may also be possible in a few years.

(2) An IR spectrum, even at low resolution, preferably using adaptive optics, should identify and provide quantitative information on the putative M dwarf in this system.

(3) The most useful optical observations may be to continue to monitor the CEN spectrum to see whether evidence for a variation in nebular density occurs.

(4) The variability of the MIR component needs to be investigated further, hopefully by repeating observations with *Spitzer*. A spatially resolved MIR image may become possible with the launch of the *James Webb Space Telescope*. Certainly further study of the MIR spectrum will be possible with *JWST*.

(5) The modelling of the nebula, as done over 20 years ago by DL, needs to be repeated with all the new observational data.

Support for this work was provided by NASA through grant number GO-2570 from the

Space Telescope Science Institute, which is operated by AURA, Inc., under NASA contract NAS 5-26555. We thank Drs. John Biegging and Jay Holberg for help with logistics, and Astronaut/Professor Steve Hawley for pointing out Tol 26.

Facilities: Hubble Space Telescope (WF/PC1, WFPC2), MMT

REFERENCES

- Bilíková, J., Chu, Y.-H., Gruendl, R. A., Su, K.Y.L., & De Marco, O. 2012, *ApJS*, 200, 3
- Bond, H.E. 1993, in *White Dwarfs: Advances in Observation and Theory*, NATO ASI, Series C, ed. M.A. Barstow, (Dordrecht: Kluwer) vol. 403, p. 85.
- Bond, H.E. 2009, *J. Phys.: Conf. Ser.* vol. 172, Number 1, 012029
- Bond, H.E., Ciardullo, R., & Meakes, M. G. 1993, *Planetary Nebulae*, Proc. IAU Symp. 155, eds. R. Weinberger & A. Acker, (Kluwer Acad. Publ.: Dordrecht), v. 155, p. 397
- Bond, H.E., Liebert, J.W., Renzini, A., & Meakes, M.G. 1992, in *Science with the Hubble Space Telescope*, Proc. of a ST-ECF/STScI Workshop, ESO Conference and Workshop Proceedings, No. 44, Garching near Munich: European Southern Observatory, eds. P. Benvenuti and T.J. Schreier, p. 139
- Bond, H.E., Meakes, M.G., Liebert, J. W., & Renzini, A. 1993, *Planetary Nebulae*, Proc. IAU Symp. 155, eds. R. Weinberger & A. Acker, (Kluwer Acad. Publ.: Dordrecht) p. 499.
- Bond, H. E., Pollacco, D. L., & Webbink, R.F. 2003, *AJ*, 125, 260
- Boumis, P., Paleologou, E.V., Mavromatakis, F., & Papamastorakis, J. 2003, *MNRAS*, 339, 735
- Chu, Y.-H., et al. 2011, *AJ*, 142, 75
- Ciardullo, R., Bond, H.E., Sipior, M.S., et al. 1999, *AJ*, 118, 488
- Coleman, G.D., & Worden, S.P. 1976, *ApJ*, 205, 475
- Dopita, M.A., & Liebert, J. 1989, *ApJ*, 347, 910 (DL)
- Ellis, G.L., Grayson, E.T., & Bond, H.E. 1984, *PASP*, 96, 283 (EGB)

- Ferguson, D.H., Liebert, J., Cutri, R., Green, R.F., Willner, S.P., Steiner, J.E., & Tokarz, S. 1987, ApJ, 316, 399
- Fleming, T.A., Liebert, J., & Green, R.F. 1986, ApJ, 308, 176
- Frew, D.J., & Parker, Q.A. 2010, PASA, 27, 129
- Fulbright, M.S., & Liebert, J. 1993, ApJ, 410, 275
- Gianninas, A., Bergeron, P., Dupuis, J., & Ruiz, M.T. 2010, ApJ, 720, 581 (G10)
- Gianninas, A., Bergeron, P., & Ruiz, M.T. 2011, ApJ, 743, 138
- Green, R.F., Schmidt, M., & Liebert, J. 1986, ApJS, 61, 305
- Hawley, S.A. 1981, PASP, 93, 93
- Holberg, J.B., & Bergeron, P. 2006, AJ, 132, 1221
- Ireland, M.J. et al. 2007, ApJ, 662, 651
- Jacoby, G.H., & van de Steene, G. 1995, AJ, 110, 1285
- Jeffries, R.D., & Stevens, I.R. 1996, MNRAS, 279, 180
- Liebert, J., Bergeron, P., & Holberg, J.B. 2005, ApJS, 156, 47
- Liebert, J., Bond, H.E., Dufour, P., & Ciardullo, R. 2013, in *18th European White Dwarf Workshop*, August 13-17, 2012, in Krakow, Poland, ed. J. Krzesiński, ASP Conf. Ser., in press.
- Liebert, J., Green, R., Bond, H.E., et al. 1989, ApJ, 346, 251
- Miszalski, B., Boffin, H.M.J., Frew, D.J., et al. 2012, MNRAS, 419, 39
- Miszalski, B., Mikoćajewska, J., Köppen, J., Rauch, T., Acker, A., Cohen, M., Frew, D.J., Moffat, A.F.J., Parker, Q.A., Jones, A.F., & Udalski, A. 2011, A&A, 528, A39
- Nota, A., Jędrzejewski, R., Voit, M., & Hack, W. 1996, FOC Instrument Handbook Version 7.0 (Baltimore: STScI)

- O'Dell, C.R., Balick, B., Hajian, A.R., Henney, W.J., & Burkert, A. 2002, *AJ*, 123, 3329
- Osterbrock, D.E. 1974, in *Astrophysics of Gaseous Nebulae*, (San Francisco: Freeman)
- Osterbrock, D.E. 1989, in *Astrophysics of Gaseous Nebulae and Active Galactic Nuclei*, (University Science Books: Mill Valley CA)
- Schlaafy, E.F., & Finkbeiner, D.P. 2011, *ApJ*, 737, 103
- Schlegel, D.J., Finkbeiner, D.P., & Davis, M. 1998, *ApJ*, 500, 525
- Seaton, M.J. 1979, *MNRAS*, 187, 73p
- Siegel, M.H., Hoversten, E., Bond, H.E., Stark, M., & Breeveld, A.A. 2012, *AJ*, 144, 65
- Smith, M.G., Aguirre, C., & Zemelmann, M. 1976, *ApJS*, 32, 217
- Su, K., Bilíková, J., Chu, Y.-H., et al. 2011, in *Asymmetric Planetary Nebulae 5*, Jodrell Bank Centre for Astrophysics, eds. A.A. Zijlstra, F. Lykov, E. Lagadec, & J. McDonald, p. 1.
- Su, K.Y.L., Chu, Y.-H., Rieke, G.H., et al. 2007, *ApJ*, 657, L41
- Tweedy, R.W., & Kwitter, K.B. 1996, *ApJS*, 107, 255
- Veeder, G.J. 1974, *AJ*, 79, 1056
- Wachter, S., Hoard, D.W., Hansen, K.H., Wilcox, R.E., Taylor, H.M., & Finkelstein, S.L. 2003, *ApJ*, 586, 1356
- Wood, B.E., Linsky, J.L., Müller, H.-R., & Zank, G.P. 2001, *ApJ*, 547 L49
- Wood, B.E., Müller, H.-R., Zank, G.P., & Linsky, J.L. 2002, *ApJ*, 574, 412
- Zacharias, N., Finch, C.T., Girard, T.M., Henden, A., Bartlett, J.L., Monet, D.G., & Zacharias, M.I. 2012, *UCAC4 Catalog*, VizieR On-line Data Catalog: I/322. (see also SIMBAD)

Zuckerman, B., Becklin, E.E., & McLean, I.S. 1991, in *Astrophysics with Infrared Arrays*,
ASP Conf. Series, vol. 14, ed. R. Elston, (San Francisco: ASP), p. 161

Table 1. *HST* Imaging Observations of EGB 6

| Date | Camera | Filter or Grating | Image Scale ["/pix] | Exposure [s] | Program ID & PI |
|-------------|------------------|----------------------|------------------------|-----------------|-----------------|
| 1991 Dec 2 | FOC <i>f</i> /96 | F486N ($H\beta$) | 0.022 | 693 | GO-2570/Bond |
| 1991 Dec 2 | FOC <i>f</i> /96 | F501N ([O III]) | 0.022 | 796 | GO-2570/Bond |
| 1993 Feb 3 | WF/PC1/P6 | F555W (<i>V</i>) | 0.044 | 2×100 | GO-4778/Bond |
| 1993 Feb 3 | WF/PC1/P6 | F785LP (<i>I</i>) | 0.044 | 2×500 | GO-4778/Bond |
| 1993 Apr 20 | WF/PC1/P6 | G450L | 0.044 | 3×1200 | GO-4778/Bond |
| 1993 Apr 20 | WF/PC1/P6 | G800L | 0.044 | 3×1800 | GO-4778/Bond |
| 1993 Dec 1 | WF/PC1/P6 | F555W (<i>V</i>) | 0.044 | 200 | SNAP-4308/Bond |
| 1993 Dec 1 | WF/PC1/P6 | F785LP (<i>I</i>) | 0.044 | 1000 | SNAP-4308/Bond |
| 1995 Oct 11 | WFPC2/PC | F555W (<i>V</i>) | 0.046 | 80, 160 | SNAP-6119/Bond |
| 1995 Oct 11 | WFPC2/PC | F814W (<i>I</i>) | 0.046 | 350, 500 | SNAP-6119/Bond |

Table 2. Astrometry of the EGB 6 Companion Object

| Date | Separation ["] | PA (J2000) [°] |
|-----------|-------------------|-----------------|
| 1991.9198 | 0.173 ± 0.009 | 266.3 ± 1.7 |
| 1993.0942 | 0.156 ± 0.009 | 268.9 ± 1.7 |
| 1995.7768 | 0.162 ± 0.009 | 269.6 ± 1.7 |

Table 3. EGB 6 Emission-Line Fluxes [10^{-15} erg cm $^{-2}$ s $^{-1}$]

| Ion | Wavelength [Å] | Flux, L89 | Flux, MMT 2007 | Notes |
|--------------------------|----------------|-----------|----------------|-------|
| [O II] | 3727 | <1.2 | – | 1 |
| H9 | 3835 | – | 0.2: | |
| [Ne III] | 3869 | 9.1 | 7.7 | |
| H8 | 3889 | – | 0.8 | |
| He ϵ + [Ne III] | 3970 | – | 3.4 | |
| [S II] | 4076 | <0.9 | – | 1 |
| H δ | 4101 | 1.7 | 1.2 | |
| H γ | 4340 | 3.2 | 1.9 | |
| [O III] | 4363 | 3.8 | 3.7 | |
| He I | 4471 | 0.6: | 0.4 | |
| He II | 4686 | 0.5: | 0.7 | 2 |
| [Ar IV] | 4712 | 1.3 | ?? | 3 |
| [Ar IV] | 4740 | 0.5: | ?? | |
| H β | 4861 | 6.8 | 4.7 | 2 |
| [O III] | 4959 | 11.7 | 9.2 | 1 |
| [O III] | 5007 | 37.5 | 27.1 | 1 |
| He I | 5876 | 1.1 | – | |
| [O I] | 6300 | 1.4 | – | |
| H α | 6563 | 18.2 | – | |
| He I | 6678 | 0.5: | – | |
| [S II] | 6717,6731 | <0.7 | – | 1 |

Table 3—Continued

| Ion | Wavelength [\AA] | Flux, L89 | Flux, MMT 2007 | Notes |
|--------|-----------------------------|-----------|----------------|-------|
| [O II] | 7325 | 0.8: | – | |

Note. — (1) measured flux partially or totally quenched due to high density; (2) measured flux in L89 are reduced by photospheric absorption and have not been corrected; (3) possible blend of [Ar IV] and He I.

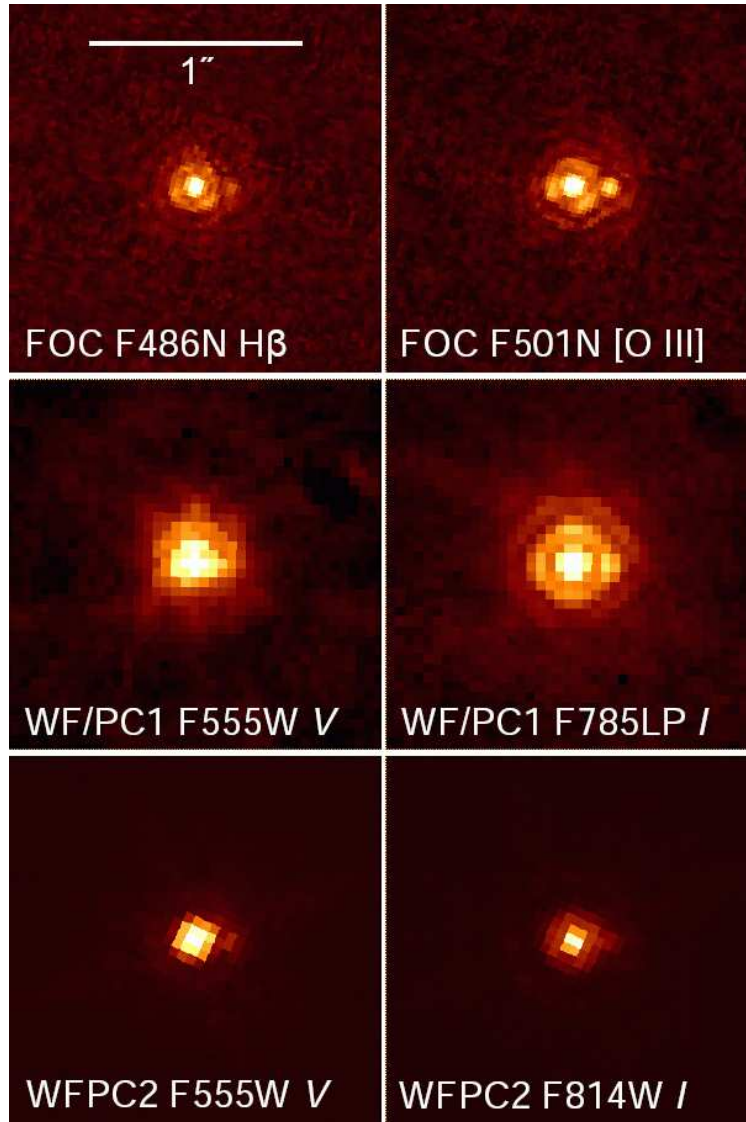


Fig. 1.— *HST* images of the central star of EGB 6. North is at the top and east on the left in all images, and each frame is $1''.75 \times 1''.75$. **Top row:** Faint Object Camera images taken in 1991 in narrow-band filters isolating H β and [O III] 5007 Å. The bright star is the hot white dwarf central star, which is accompanied by an emission-line companion located almost directly west. **Middle row:** Wide Field/Planetary Camera 1 images taken in 1993 in broad-band “V” and “I” filters. The cool dM companion is detected in the *I* filter at the location of the CEN. **Bottom row:** Wide Field and Planetary Camera 2 images taken in 1995 in broad-band “V” and “I” filters. The companion star is again detected, but is fainter in *I* due to a narrower bandpass, as discussed in the text.

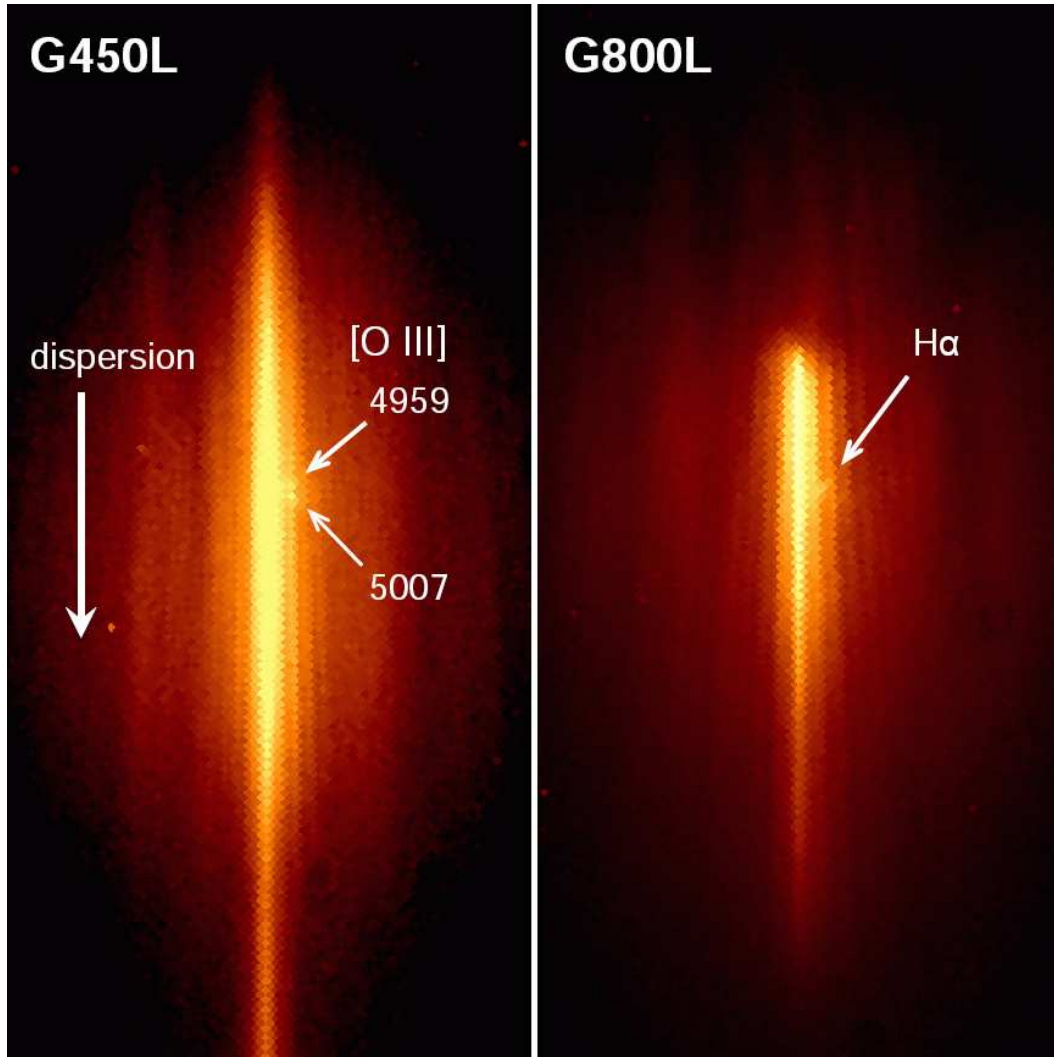


Fig. 2.— *HST* grism images, obtained with WF/PC1 in 1993. Both images were taken at a telescope roll angle that maximized the spatial separation of the faint companion from the hot white dwarf. **Left:** G450L image, showing the intense blue spectrum of the hot central star. The companion is detected only at the [O III] 4959 and 5007 Å nebular emission lines. **Right:** G800L image, showing the red continuum of the white dwarf. The companion is detected only at the H α emission line. See text for further discussion.

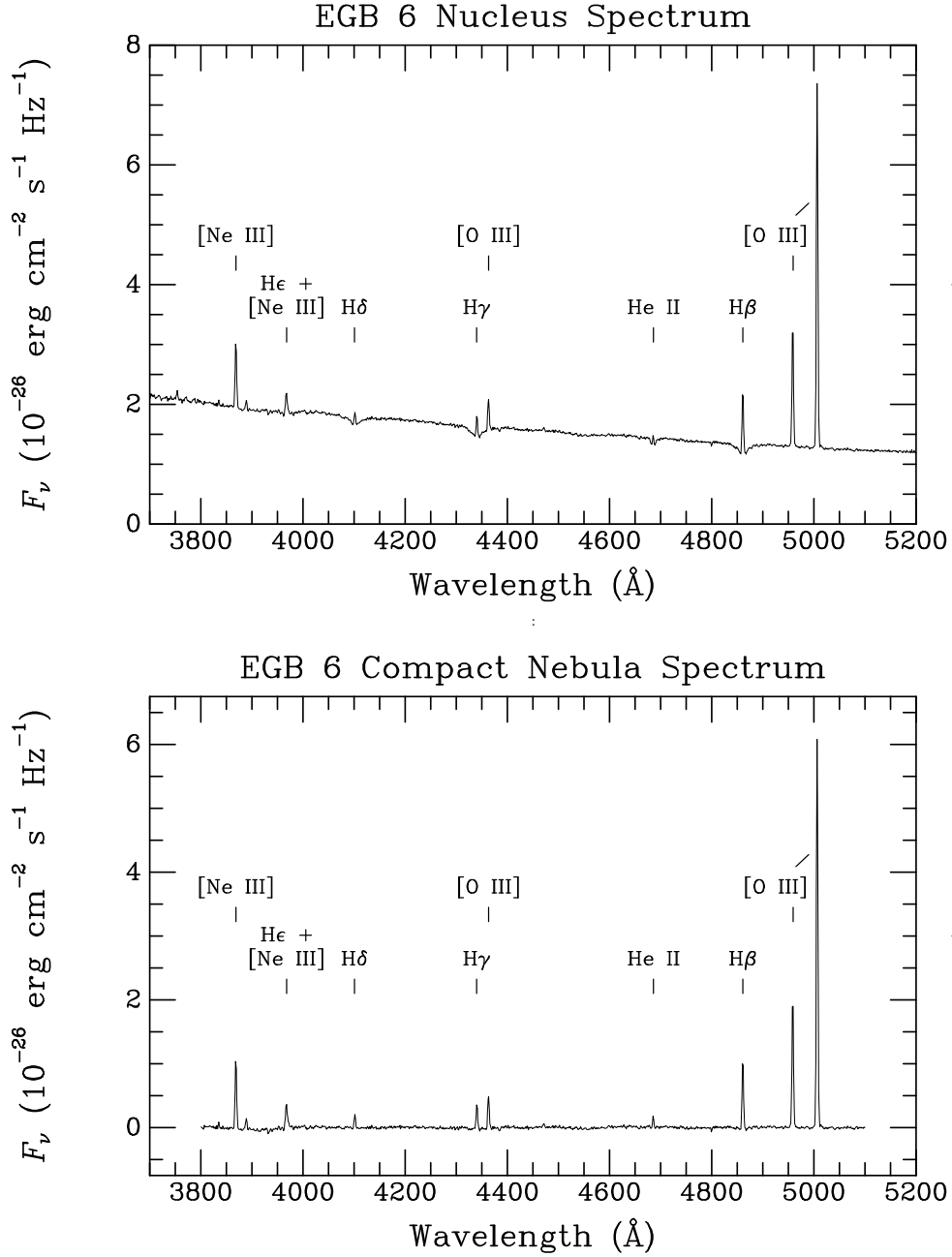


Fig. 3.— **(top)** Spectrum of the central star of EGB 6 from the 2007 6.5-m MMT observation, showing the photospheric spectrum of the DAOZ nucleus with superposed CEN. **(bottom)** Emission-line spectrum of the CEN, obtained by subtracting the best-fitting model-atmosphere WD synthetic spectrum (Gianninas et al. 2010, G10), as described in the text.

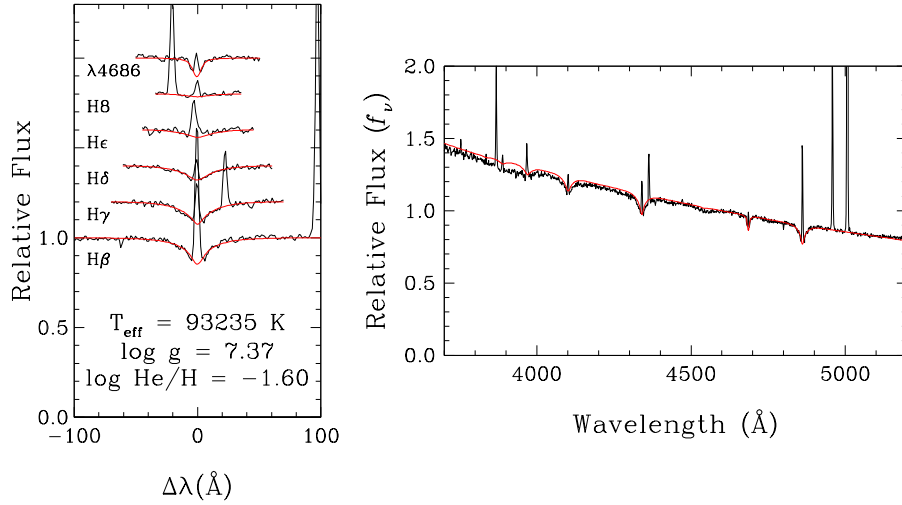


Fig. 4.— **(Left)** Detailed fits to the He II and individual Balmer absorption lines with the blended CEN emission lines omitted from the fitting procedure. The synthetic spectrum fit to the lines is shown as the red curve. **(Right)** Superposition of the spectroscopic solution (red) to entire blue spectrum, both normalized to a continuum set to unity at 4600 Å.